Understanding the Self-Assembly of Proteins onto Gold Nanoparticles and Quantum Dots Driven by Metal-Histidine Coordination

Fadi Aldeek, Malak Safi, Naiqian Zhan, Goutam Palui, and Hedi Mattoussi*

Department of Chemistry and Biochemistry, Florida State University, 95 Chieftan Way, Tallahassee, Florida 32306, United States

ABSTRACT Coupling of polyhistidine-appended biomolecules to inorganic nanocrystals driven by metal-affinity interactions is a greatly promising strategy to form hybrid bioconjugates. It is simple to implement and can take advantage of the fact that polyhistidine-appended proteins and peptides are routinely prepared using well established molecular engineering techniques. A few groups have shown its effectiveness for coupling proteins onto Zn- or Cd-rich semiconductor quantum dots (QDs). Expanding this conjugation scheme to other metal-rich nanoparticles (NPs) such as AuNPs would be of great interest to researchers actively seeking effective means for interfacing nanostructured materials with biology. In this report, we investigated the metal-affinity driven self-assembly between AuNPs and two engineered proteins, a His_7-appended maltose binding protein (MBP-His) and a fluorescent His_6-terminated mCherry protein. In particular, we investigated the influence of the capping ligand affinity to the nanoparticle surface, its density, and its lateral extension on the AuNP-protein self-assembly. Affinity gel chromatography was used to test the AuNP-MPB-His_7 self-assembly, while NP-to-mCherry-His_6 binding was evaluated using fluorescence measurements. We also assessed the kinetics of the self-assembly between AuNPs and proteins in solution, using time-dependent changes in the energy transfer quenching of mCherry fluorescent proteins as they immobilize onto the AuNP surface. This allowed determination of the dissociation rate constant, $K_d^{-1} \sim 1-5$ nM. Furthermore, a close comparison of the protein self-assembly onto AuNPs or QDs provided additional insights into which parameters control the interactions between imidazoles and metal ions in these systems.

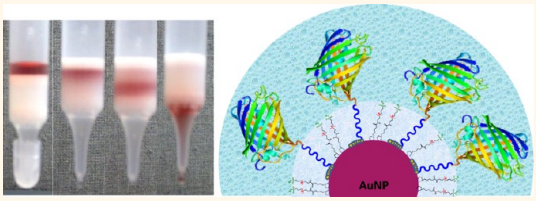

KEYWORDS: gold nanoparticles · luminescent quantum dots · polyhistidine · metal-affinity interactions · self-assembly · kinetics · energy transfer · affinity chromatography

Biologically active platforms prepared by combining biomolecules with nanocrystals that exhibit unique photophysical properties have attracted much interest in the past decade.[1−8] Such hybrid platforms offer a great potential for use in a variety of biosensing and imaging applications.[2,7,9−11] They require effective and controlled conjugation with chemical or biological vectors, such as proteins, peptides, and nucleic acids.[2,7,9] A few coupling strategies have been developed in the past few years to achieve this goal, including covalent attachment *via* carbodiimide, maleimide or click chemistry.[7,12−14] A greatly promising strategy that is rather simple to implement involves the direct coordination between proteins or peptides appended with a C- or N-terminal polyhistidine sequence (His_n tag) and metal-rich inorganic nanoparticles. Such approach has been applied to hydrophilic CdSe-ZnS core−shell QDs, with a reported dissociation constant of $K_d^{-1} = 1-10$ nM.[15] However, metal-His driven self-assembly of protein onto QDs is strongly dependent on the nature and lateral extension of the ligands used to confer water solubility to the nanocrystals.[15−17]

Expanding this conjugation scheme to other metal-rich nanoparticles (NPs) would be of great interest to researchers actively seeking conjugation of biomolecules to various inorganic NPs. In particular, functionalized noble-metal NPs would be ideally suitable for such mode of self-assembly. Among these systems gold and silver NPs are very attractive, because of their inert nature and size-tunable optical and electronic properties.[18−20] Gold NPs (AuNPs) have been intensively studied by numerous groups, with the aim of developing active

* Address correspondence to mattoussi@chem.fsu.edu.

Received for review August 27, 2013 and accepted October 17, 2013.

Published online October 17, 2013
10.1021/nn404479h

platforms that have great potential for use in sensing and therapy.[19−24] In addition, AuNPs and clusters provide efficient quenchers of organic dye and QD emission when brought in close proximity.[25−27] For instance, AuNP-dye pairs have been used in assay design to sense binding events and oligonucleotide hybridization based on energy transfer interactions.[25,28−30]

Thus far, only a few groups have investigated the use of imidazoles as means to drive ligation of biomolecules onto AuNPs.[31,32] For example, Strouse, Logan, and co-workers prepared 1.5 nm AuNPs stabilized with bis(*p*-sulfonatephenyl)phenylphosphine (bSPP) or triphenylphosphine (TPP), which were then cap-exchanged with peptides appended with varying length polyhistidine tags (peptide-His_n, with n = 2, 6, 10). They used NMR and FT-IR spectroscopy to probe the coordination of the histidine groups (in the peptide) onto the AuNPs.[31] They subsequently showed that a His_6-appended full size protein (human acidic fibroblast growth factor, FGF1) can bind onto a Au nanoparticle. More precisely, they probed the time-dependent conformational changes of FGF1 mutant during the self-assembly of the protein onto 1.5 nm AuNPs passivated with compact zwitterionic peptide.[32] NMR, though effective, often requires rather high reagent concentrations, because of its low sensitivity as a spectroscopic technique. More recently, Krull and co-workers reported that a substrate functionalized with a poly(acrylic acid) (PAA) modified with a few imidazoles can permit capture and immobilization of citrate-stabilized AuNPs, a process attributed to binding of the imidazole groups to the NPs.[33] In these examples, the common feature was the use of weakly bound ligands on the AuNPs prior to attempting the metal-His coupling.

In this report, we investigate the metal-affinity coordination of polyhistidine-appended proteins onto AuNPs that have been prepared with distinctly different ligands. We tuned the affinity of the ligand to the NPs, its density, and its lateral extension, and tested the importance of these parameters to the self-assembly between AuNPs and polyhistidine-tagged proteins. We systematically probed the self-assembly of AuNPs with His_7-appended maltose binding protein (MBP-His_7) and fluorescent His_6-teminated mCherry protein. The NPs were capped with a few sets of ligands that exhibit distinctly different surface-affinities to the Au surface (namely, citrate, lipoic acid (LA), LA-appended with a zwitterion or a polyethylene glycol segment); for the LA-based ligands we varied the ligand density and lateral size. This allowed us to probe when metal-His interactions with Au-rich NPs takes place and what exactly controls those interactions. We used affinity chromatography to test the AuNP-MPB-His_7 self-assembly, while NP-to-mCherry-His_6 binding was tested using energy transfer quenching. We found that the His-conjugation can indeed be applied to AuNPs, with strong binding rate constants. We also found that because such coupling requires direct coordination between the imidazole moieties and the Au-rich surfaces, several other parameters play important roles, namely, ligand affinity to the NP surface, size, and density.

RESULTS AND DISCUSSION

One of our motivations is to explore the versatility of the conjugate self-assembly promoted by metal-affinity driven interactions between the surface of inorganic nanocrystals and polyhistidine-tagged biomolecules. Indeed we and others have shown that polyhistidine-tagged proteins and peptides can tightly self-assemble onto CdSe and ZnS-overcoated QDs.[34−37] Those studies have also shown that such conjugation requires direct access of the histidine tag to the metal-rich QD surfaces. This has limited implementation of this strategy only to QDs capped with compact ligands, namely, DHLA and zwitterion-modified DHLA ligands.[38−40] For example, conjugation of His-tagged-proteins (globular in nature) onto DHLA-PEG-capped QDs was found to be highly inefficient because of the steric hindrance imposed by the PEG coating.[15] However, introduction of a long flexible linker between the His-tag and protein allowed the use of nanocrystals capped with PEGylated ligands.[41] Conjugation of peptide-His was applied to both DHLA- and DHLA-PEG-capped-QDs because of the peptide more extended conformation.[15] However, application of such conjugation to other inorganic nanocrystals was very limited in scope. For example, conjugation to AuNPs was reported by two groups, and only NPs originally functionalized with weakly bound ligands (namely, citrate, bis(*p*-sulfonatephenyl)phenylphosphine, bSPP, or triphenylphosphine, TPP) were used.[31,33]

In this study, we would like to prove that metal-affinity driven self-assembly can effectively be applied to AuNPs, and gain further insights into what controls such self-assembly as applied to AuNPs and ZnS-overcoated QDs. In particular, we would like to delineate the importance of ligand affinity to the metal surface of the nanoparticles, its nature, size, and density to the effectiveness of the metal-His interactions in general. One important issue we will try to address can be formulated as follows: How does the specific nature of the capping ligands affect the His-mediated binding? Do the imidazole groups driving the coupling of the biomolecules compete with the ligand for coordination to the metal surface of the NPs, or interactions occur independent of the ligand used? For this we used AuNPs and QDs capped with a similar set of ligands, namely, lipoic acid and lipoic acid appended with either a zwitterion or a short polyethylene glycol segment (LA, LA-ZW and LA-PEG). The QDs were prepared in hydrophobic media, *via* hot injection techniques, and transferred to buffer media using a

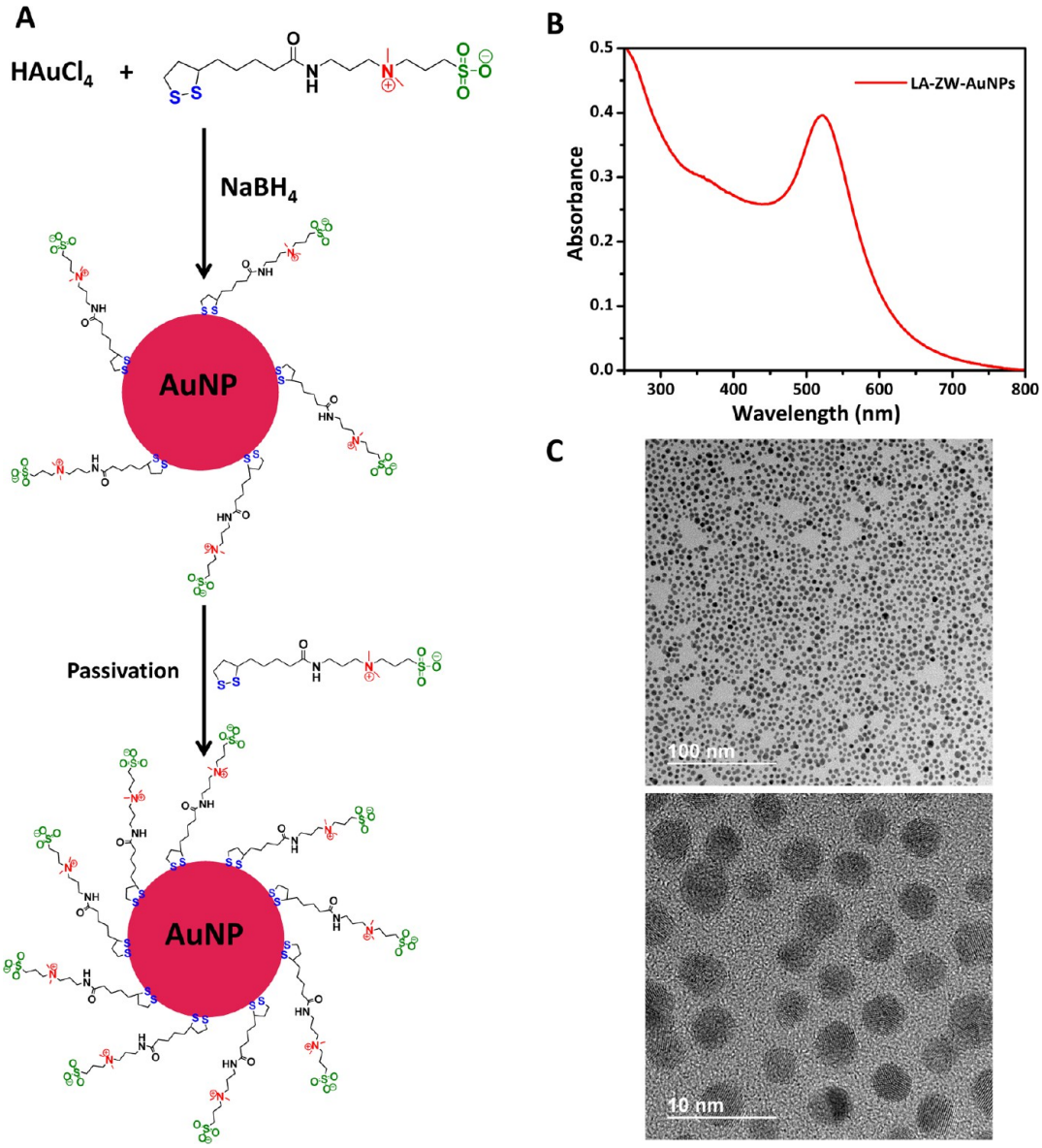

Figure 1. (A) Schematic representation of the one phase growth of AuNPs using LA-ZW ligand. (B) UV−vis absorption spectrum of 5 nm AuNPs capped with LA-ZW; the Au:ligand molar ratio used for the synthesis was 90:1. (C) TEM images of the AuNPs prepared above using LA-ZW.

photoligation strategy with LA-ZW and LA-PEG, as previously described.[40,42] Conversely, the AuNPs were prepared in aqueous phase using $NaBH_4$-reduction, where *in situ* reduction of the Au precursor, growth, and functionalization with the ligands can be achieved.[43,44] In addition to tuning the NP size, this route allowed control over the ligand density on the final NPs. We prepared 5 nm AuNPs using Au-to-ligand molar ratio of 90:1 (excess metal ions), and a growth period of 3 h.[43] The as-prepared NPs have sparse ligand coverage (*i.e.*, are "partially passivated"). However, an additional passivation step, originally introduced to increase coverage of the NP surface and enhance colloidal stability,[43] can be used to vary the final ligand density on the nanoparticles. The latter was gradually varied by increasing the amount of ligands added in the extra passivation step, using final molar ratios of 90:1, 50:1, 25:1, 5:1, 2:1, and 1:1. For instance, LA-ZW-AuNPs prepared with final molar ratios of 5:1, 2:1, and 1:1 will be referred to as "passivated", while those prepared with higher ratios will be referred to as "partially passivated" (Figure 1A). We applied this strategy to prepare LA-, LA-ZW- and LA-PEG_{750}-OCH_3-capped AuNPs. We also prepared 5 nm citrate-AuNPs and used them as control materials. The UV−vis absorption spectra of the LA-, LA-ZW-, LA-PEG- and citrate-stabilized AuNPs show a typical plasmonic peak with narrow plasmon bandwidth, centered at 520 nm (Figure 1B). The structure of the AuNPs was also characterized by transmission electronic microscopy (TEM). Typical medium and high magnified TEM images of the AuNPs stabilized with LA-ZW collected after synthesis

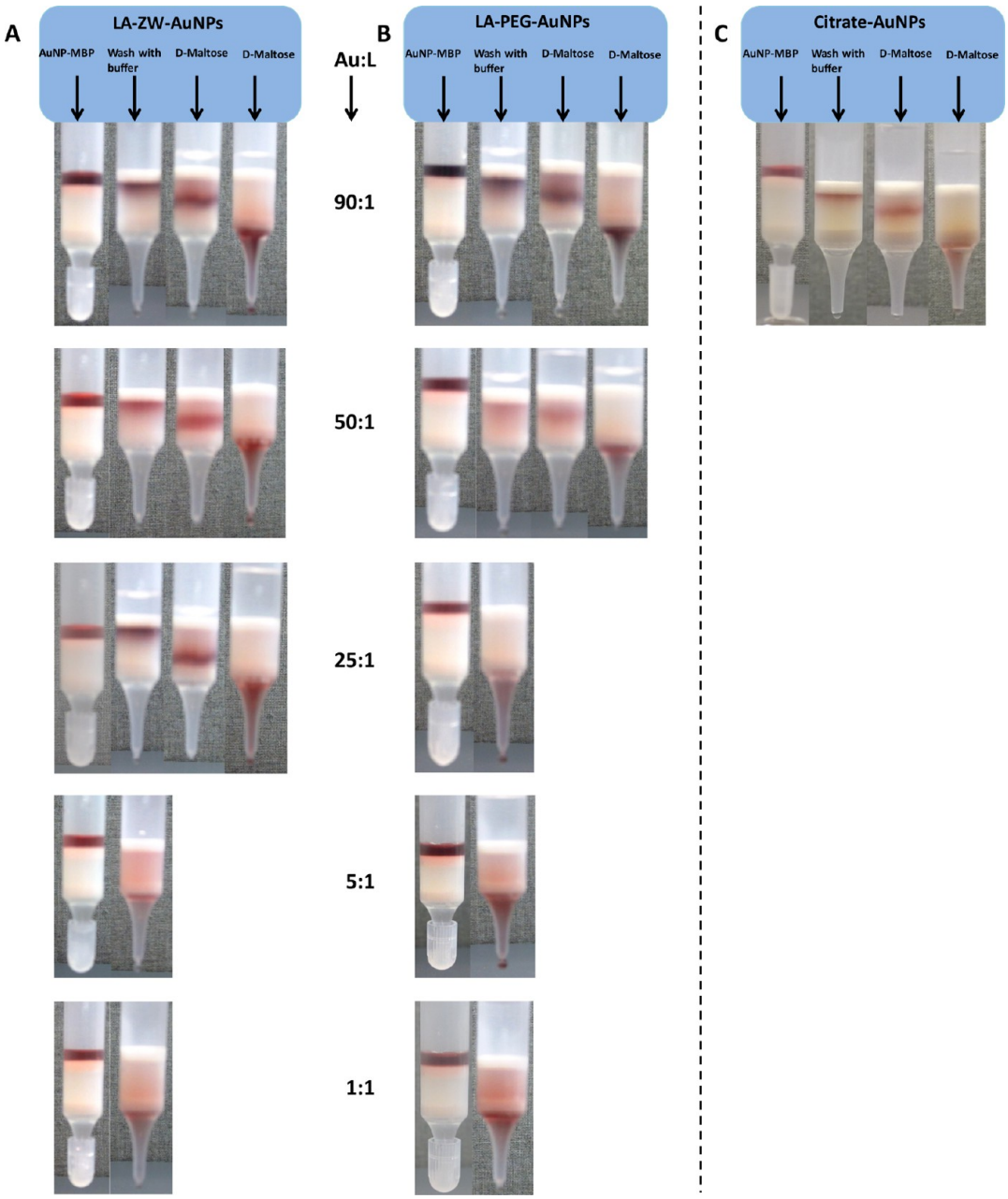

Figure 2. Affinity chromatography test of AuNP-MBP-His_7 self-assembly: binding onto amylose column and release with added maltose. The AuNPs are capped with either LA-ZW (A) or LA-PEG_{750}-OCH_3 (B) and were originally prepared using Au:ligand molar ratio of 90:1, followed by an extra passivation step with different amounts of ligand to reach a final Au:ligand ratio of 90:1, 50:1, 25:1, 5:1, 2:1, and 1:1. Panels from top to bottom correspond to AuNPs with increasing ligand density. No binding to amylose was measured for mixtures of proteins with NPs prepared with Au:LA-ZW = 5:1, 2:1, and 1:1 or with Au:LA-PEG = 25:1, 5:1, 2:1, and 1:1. (C) Test using a mixture of citrate-AuNPs and MBP-His_7, confirming conjugate formation.

and purification are shown in Figure 1C. Images show homogeneous nanoparticles with an average diameter of 5 $\pm$ 0.5 nm.

Self-Assembly of MBP-His_7 onto AuNPs. The first test of AuNP-to-protein self-assembly relied on affinity chromatography and probed the competition between the binding of MBP to an amylose gel and to its substrate, maltose, in solution. Following an incubation time of 45 min at 4 °C, the AuNP and MBP-His_7 mixture was loaded onto a column filled with amylose gel, and using the natural pinkish color of the AuNPs, we tracked when binding to the column followed by release with added maltose takes place and when it does not; here, the protein allowed specific interaction of the conjugate with the amylose gel while the AuNPs provided a visual means for tracking their localization. Figure 2 shows that binding to amylose, as indicated by the buildup of a pinkish band on the top of the column(s), takes place only when AuNPs partially passivated with the LA-modified ligands are used. The band stays intact after several washes with buffer, but is easily eluted when a few milliliters of 20 mM

D-(+)-maltose solution are added. This indicates that AuNP-MBP-His_7 self-assembly has taken place for these NPs. Figure 2 also shows that upon increasing the number of ligands per AuNP (increased passivation), binding to the gel column is decreased until completely prevented. For those mixtures the pinkish band never builds up and materials are fully displaced during the washing step. Overall, we found that binding to amylose and release by maltose takes place for partially passivated AuNPs with compact LA-ZW ligands (*i.e.*, using a final Au-to-ligand molar ratio of 90:1, 50:1, and 25:1). Conversely, passivated AuNPs, prepared with a final Au-to-ligand molar ratio of 5:1, 2:1, and 1:1 do not bind to the column, indicating that AuNP-to-MBP-His_7 self-assembly has not taken place (Figure 2A).

Self-assembly onto PEGylated-AuNPs is even more sensitive to the amount of ligands used. For instance, NPs that were partially passivated using a final Au:ligand ratio of 90:1 exhibit the signatures of conjugate formation with binding onto the amylose column and release with added maltose (Figure 2B). However, for Au:ligand ratio of 50:1, the binding was found to be partial, while for Au:ligand ratio of 25:1 or lower, the NPs were rapidly eluted after loading onto the column, indicating absence of AuNP-MBP-His_7 conjugate formation. To discard the possibility that excess free ligands in the medium may be interfering with the conjugation for dispersions of fully passivated NPs (*e.g.*, a final Au:LA-ZW = 1:1), we applied 6 rounds of purification using a membrane filtration device to those dispersions, before mixing with MBP. None of these mixtures exhibited binding onto the amylose column (data not shown).

AuNPs grown in the presence of lipoic acid overall showed similar behavior to that observed for LA-ZW-capped NPs, where biologically active conjugates were formed only for partially passivated NPs (*i.e.*, prepared with Au:ligand ratio exceeding 25:1, data not shown). Nonetheless, these dispersions exhibited a minor difference: we found that for MBP-His mixed with fully passivated LA-AuNPs a very small fraction of the loaded AuNPs bound to the column and was release by maltose; most of the pink solution of AuNPs readily eluted upon loading onto the column (see Supporting Information Figure 1S). We attribute this to potential electrostatic interactions between the protein and carboxy groups on the NPs.

We also tested the self-assembly of MBP-His onto LA-ZW-AuNPs prepared *via* ligand exchange starting with 5-nm citrate-capped NPs. Following ligand exchange, the dispersion was divided into separate aliquots, and each was further purified from excess free ligands using varying rounds of concentration/dilution using a membrane filtration device (with a molecular weight 50 kDa M_w cutoff), to allow varying degrees of free ligand removal from the dispersions; the number of rounds varied from one aliquot to another. The AuNPs were tested for their ability to bind to MBP-His_7 using the above amylose affinity chromatography. No self-assembly between MBP and these LA-ZW-AuNPs (prepared *via* ligand exchange) was observed for any of those aliquots (Figure 3).

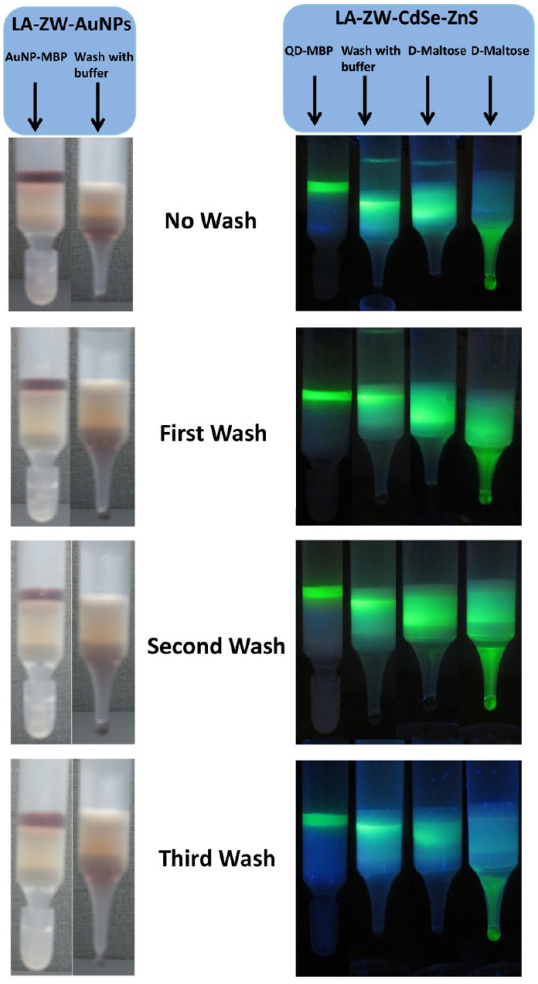

Figure 3. Side-by-side affinity chromatography tests/assays (binding to amylose and release with maltose) applied to AuNPs (left panel) and luminescent QDs (right panel) after successive purifications from excess free ligands; the nanocrystals were mixed with MBP-His_7 (NP-to-MBP-His_7 molar ratio = 1:10). The LA-ZW-AuNPs were prepared *via* cap exchange starting with citrate-stabilized AuNPs, while the QDs were photoligated with LA-ZW. Numbers of purifications using a 50 kDa membrane filtration device are shown.

When citrate-stabilized AuNPs were used, self-assembly with MBP-His_7 readily took place, as indicated by the tight immobilization onto the amylose column followed by release with maltose (see Figure 2C).

Self-Assembly of MBP-His_7 onto LA-ZW-Capped QDs. To complement the above experiments, we prepared CdSe-ZnS QDs using high temperature reduction in coordinating solvents following procedures described in the literature.[45−49] These QDs were photoligated with excess of LA-ZW ligands, as described in our recent reports.[42] The hydrophilic QD dispersion (stock solution) was divided in four separate aliquots, and each one

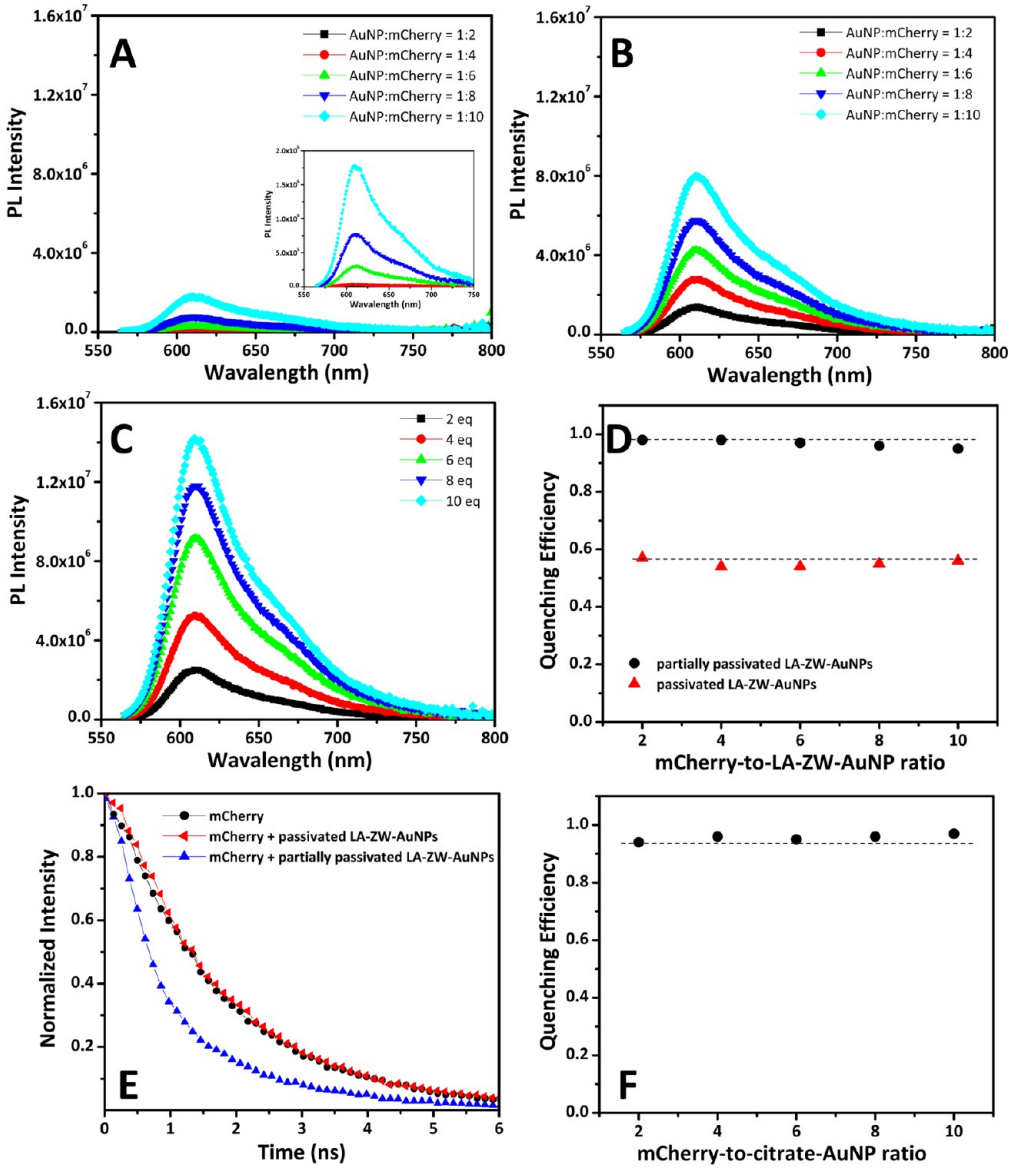

Figure 4. (A and B) PL spectra of mCherry after mixing with partially passivated and passivated LA-ZW-AuNPs, respectively. (C) Control experiment showing the PL spectra collected from mCherry alone at the molar ratios used. (D) Plots of the quenching efficiency *versus* mCherry-to-AuNP molar ratio extracted from data shown in (A) for partially passivated LA-ZW-AuNPs and in (B) for fully passivated LA-ZW-AuNPs. (E) Time-resolved fluorescence decay profiles of mCherry alone (●), mCherry mixed with passivated (♦) and partially-passivated LA-ZW-AuNPs (▲), respectively. The mCherry-to-AuNP molar ratio used was 1:1. (F) Cumulative plots of the quenching efficiency *versus* mCherry-to-AuNP molar ratio for citrate-capped AuNPs.

was subjected to a few rounds of purification using a membrane filtration device as done for LA-ZW-capped AuNPs above. Each of these dispersions was then mixed with 10 equiv of MBP-His_7, left to incubate for 45 min at 4 °C, and then subjected to the affinity chromatography test using amylose gel. The results are summarized in Figure 3. Clearly, the MBP-His_7 bind to all CdSe-ZnS QD dispersions photoligated with LA-ZW ligand, regardless of how many rounds of membrane filtrations have been applied to the dispersion. This indicates that metal-His coordination applies to fully passivated QDs, and it is not affected by the degree of excess "free" ligand potentially present in the dispersion when QDs are used.

Self-Assembly of mCherry-His_6 onto AuNPs. In the second test we took advantage of the fluorescent nature of mCherry and confirmed NP-protein conjugation using energy transfer-induced quenching of the protein emission when it self-assembles onto the AuNPs. We combined steady-state and time-resolved fluorescence measurements to evaluate the mCherry PL quenching when mixed with the various configurations of AuNPs tested above. Figure 4 shows the progression of the steady-state PL spectra collected from dispersions of AuNPs mixed with mCherry at several protein-to-NP molar ratios using partially passivated AuNPs with a final Au:LA-ZW = 90:1 (Figure 4A), passivated AuNPs with a final Au:LA-ZW = 1:1

(Figure 4B), and control solutions of mCherry alone at the corresponding molar concentrations (no AuNPs, Figure 4C). Figure 4D shows a plot of the compiled quenching efficiency, *E*, *vs* mCherry-to-AuNP ratio extracted from the fluorescence data using the expression:

$$E = 1 - \frac{F_{DA}}{F_D} \quad (1)$$

where F_{DA} and F_D designate the PL intensity measured for mCherry mixed with AuNP and mCherry alone, respectively. Pronounced changes in the mCherry PL are measured only upon mixing mCherry with either partially passivated AuNPs (*i.e.*, LA, LA-ZW or LA-PEG-capped), or citrate-stabilized NPs (Figure 4). In comparison, smaller losses are measured for mCherry mixed with fully passivated AuNPs; additional data collected using LA-PEG-AuNPs are provided in the Supporting Information (Figure S2). The time-resolved decay profiles shown in Figure 4E confirm the steady-state data and show that a significant decrease in the mCherry excited-state lifetime was measured only upon mixing mCherry with partially passivated LA-ZW-AuNPs or citrate-stabilized NPs. No decrease in mCherry lifetime was measured for mixtures of mCherry with fully passivated AuNPs. Our primary goal here is to show that steady-state and time-resolved PL data confirm that proximity-driven energy transfer quenching of mCherry occurs only when self-assembly takes place, as anticipated. A detailed analysis of the intricacies involved in the energy transfer process for these assemblies is beyond the scope of this report. They may be discussed in future studies.

Kinetics of mCherry-His$_6$ Self-Assembly onto AuNPs. In these experiments, we monitored the kinetics of the AuNP-mCherry-His$_6$ conjugate formation in solution by tracking the time-dependent changes in the mCherry fluorescence emission immediately after reagent mixing. For this we used partially passivated LA-, LA-ZW- and LA-PEG-AuNPs and citrate-stabilized AuNPs. This provided a molecular characterization of the metal-affinity-driven assembly between the AuNPs and mCherry-His$_6$. We followed the rationales used in our previous report to extract an estimate for the apparent binding rate constant (k_{app}).[15] We applied a first-order bimolecular reaction analysis to assess the kinetics of protein binding on the AuNP surfaces, where we maintained the protein-to-AuNP molar ratio fixed at 1:1 and probe the time-dependent changes in the mCherry PL for dispersions with nanoparticle concentrations ranging from 1 to 60 nM.[15]

Since we limit our experimental conditions to a small NP-to-protein ratio, the system at equilibrium is far from saturation. One can thus assume that the binding events of two distinct proteins on a NP are essentially independent, *i.e.*, AuNP-(mCherry)$_n$ + mCherry = AuNP-(mCherry)$_{n+1}$, where AuNP-(mCherry)$_n$ and AuNP-(mCherry)$_{n+1}$ designate a NP bound to *n* and *n* + 1 proteins, respectively (see scheme in Figure 5). At such small ratios, we can also assume that the binding and dissociation rates do not depend on *n*. This implies that the concentration of bound proteins follows a monoexponential decay until equilibrium is reached. As the number of self-assembled AuNP-mCherry-His$_6$ conjugates in the solution increases, the overall PL of mCherry progressively decreases due to energy transfer quenching induced by the proximal AuNPs. Thus, the kinetics of AuNP-protein self-assembly becomes more rapid when the reagent concentrations are increased. Within the framework of a first-order bimolecular reaction, we can express the time-dependent concentration of bound mCherry (BmC) proteins onto a AuNP with an expression of the form:[15]

$$[BmC](t) = [mC]_0 \times (1 - \exp(-k_{app}t)) \quad (2)$$

where $[mC]_0$ designates the initial mCherry concentration and k_{app} is the apparent binding rate. Thus, for the above experimental conditions the mCherry PL decay can be fit to an exponential decay function of the form:

$$PL_{mC}(t) = PL_{mC|0} - \Delta(PL_{mC}) \times (1 - \exp(-k_{app}t)) \quad (3)$$

Here $PL_{mC|0}$ designates the initial PL signal (prior to mixing) and $\Delta(PL_{mC})$ corresponds to the overall drop in protein emission from the initial time until saturation is reached. Figure 5A shows the time-dependent PL change of mCherry following mixing with the AuNPs. Data show that the PL decay is faster for higher reagent concentrations, as anticipated from the above model. Fitting the data to eq 3 provides values for k_{app} at each AuNP concentration. A plot of these values shows a linear increase of k_{app} with protein concentration (Figure 5B), in agreement with the dependence of k_{app} *vs* reagent concentration expected from the first-order bimolecular reaction analysis model in eq 4:[15,50]

$$k_{app} = k_{on}[mC] + k_{off} \quad (4)$$

From the above data we extract values for the dissociation rate, k_{off} (intercept at the origin) and the association rate, k_{on} (slope). These can be used to extract a measure for the equilibrium/dissociation constant $1/K_d$ (defined as $1/K_d = k_{off}/k_{on}$); the latter designates the concentration at which half of the available binding sites are occupied. The value for K_d^{-1} extracted from the above experimental data for mCherry-to-AuNP interactions is ~5 nM.

Similarly, since the self-assembly of a AuNP with one, two, or three proteins is independent and the quenching involves one-to-one interactions at equilibrium, an expression of the dissociation constant can be written as $1/K_d = [mC]_0[AuNP]/[BmC]$. Further manipulation of this relation can provide an expression relating the PL

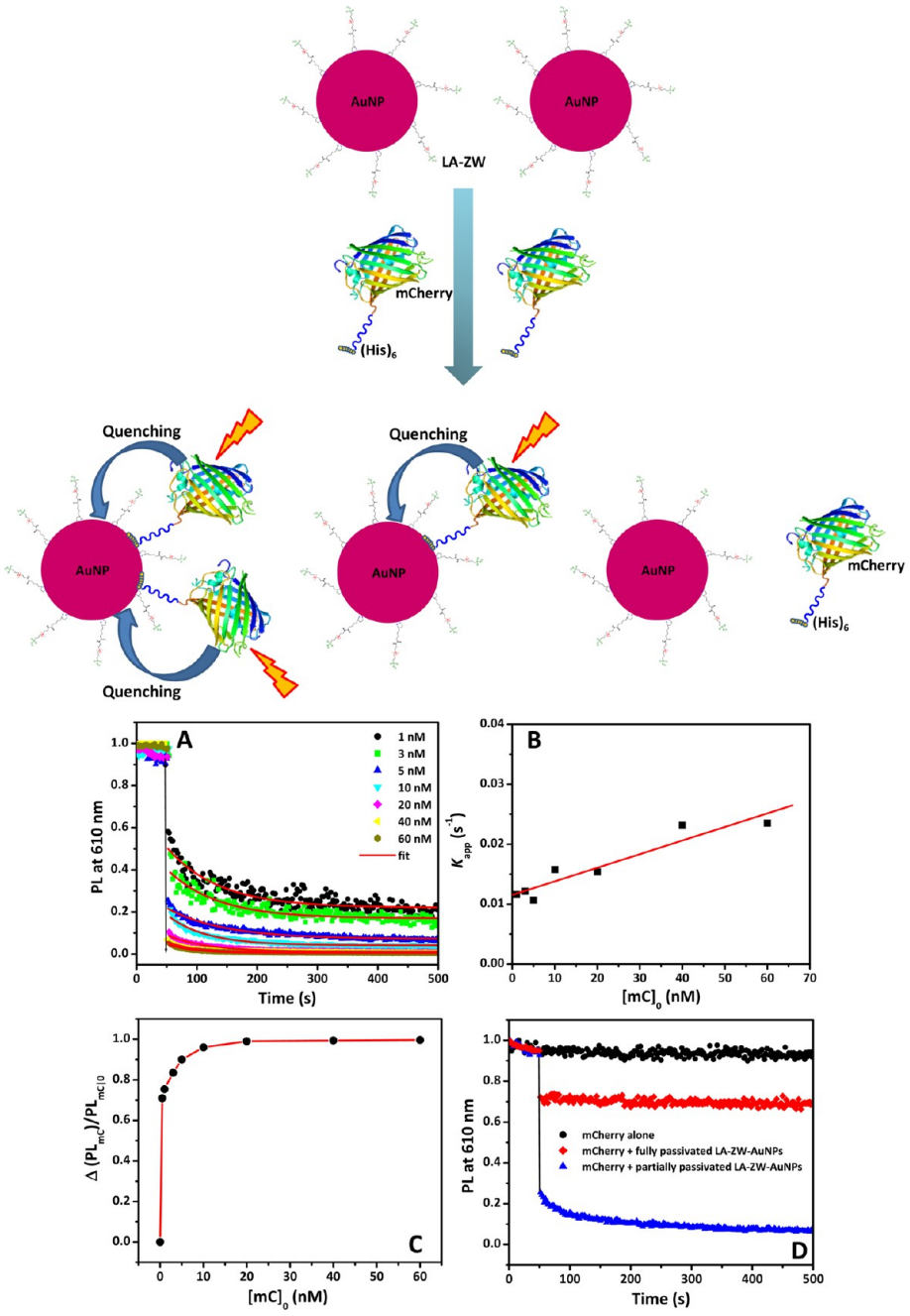

Figure 5. (Top) Schematic representation of the kinetics driving the NP-to-mCherry self-assembly. (A) Representative time-traces of mCherry PL decay after mixing with partially passivated LA-ZW-AuNPs (arrow at t = 50 s indicates the mixing of mCherry and AuNPs), normalized to its level at t = 0. Lines are fits using eq 3. (B) Apparent binding rate as a function of mCherry concentration; line is a fit to eq 4. (C) Concentration-dependent relative PL loss upon binding with AuNPs; solid line is a fit using eq 5. (D) Control experiment showing representative time-traces of mCherry PL alone (●) and mCherry mixed with fully passivated (♦) and partially passivated (▲) LA-ZW-AuNPs; the concentration in this control experiment was equal to 5 nM. The samples were excited at 587 nm, and signal was collected at 610 nm.

drop, ΔPL_{mC}, to the total mCherry concentration in the medium of the form:[15]

$$\frac{\Delta(PL_{mC})}{PL_{mC|0}} \approx \frac{[mC]_0}{K_d^{-1} + [mC]_0} \qquad (5)$$

This implies that the data shown in Figure 5C can be exploited to extract another estimate for K_d^{-1} for the self-assembly of AuNP and mCherry promoted by metal-His interactions. Given the fact that the experimental curve rapidly reaches saturation, a data fit using this expression provides an upper limit for the dissociation constant $K_d^{-1} \leq 0.3$ nM; this value is smaller than the one extracted from the exponential fit to the time-dependent decay of the mCherry emission (Figure 5A).

The solution self-assembly of mCherry-His_6 onto citrate-stabilized AuNPs showed a similar trend, but

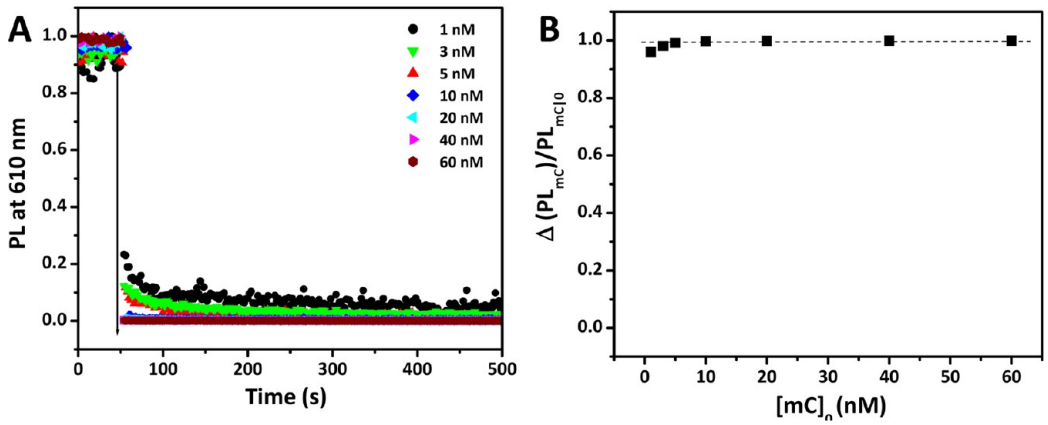

Figure 6. (A) Representative time-traces of mCherry PL decay after mixing with citrate-capped AuNPs normalized to its level at $t = 0$; the arrow at $t = 50$ s points to reagent mixing. The mCherry and AuNP concentration were varied from 1 to 60 nM (molar ratio was fixed at 1). (B) Concentration-dependent relative PL drop of mCherry upon binding with citrate-stabilized AuNPs; the line is drawn for guidance.

kinetics were substantially faster than what was seen for the self-assembly onto partially passivated LA-ZW-AuNPs (shown in Figure 5A). Data shown in Figure 6 indicate that the PL decay reached its asymptotic limit within a few second of mixing, and that the relative PL drop reached saturation at nearly all concentrations used. Here too only an upper limit for the dissociation constant can be extracted from the PL drop and eq 5 ($K_d^{-1} < 0.1$ nM).

We should note that the dissociation constant measured for the present mCherry-His and AuNP is overall comparable (*i.e.*, same order of magnitude) to the one measured for the self-assembly of MBP-$His_{5,11}$ onto DHLA-QDs ($K_d^{-1} \sim 1$ nM).[15] Because K_d^{-1} is defined as the ratio between k_{off} and k_{on}, this implies that smaller K_d^{-1} correspond to faster reaction and *vice versa*. Figure 5D shows a control experiment where the time-dependent PL measurement of the mCherry and mCherry mixed with fully passivated LA-ZW-AuNPs. Following the initial small drop in the mCherry PL signal, the measured intensity stayed constant over the full 500 s of monitoring. The absence of time-dependent decay implies that mCherry mixed with passivated AuNPs do not self-assemble on the NPs. The immediate drop in the protein signal can be attributed to solution phase-quenching. This is in agreement with the lifetime data collected above. Overall, these results show that conjugation takes place only for partially passivated and that the progression toward binding equilibrium depends strongly on the concentration of His-mCherry and AuNPs in the solution, with faster kinetics for higher concentration.

The above set of data combined proves unequivocally that self-assembly of biomolecules facilitated by metal-His coordination onto AuNPs can be implemented. It also confirms that the self-assembly involves direct interactions between the imidazole groups and the metal-rich surface of the NPs, as was shown for the binding of protein-His or His-modified polymers onto ZnS-overcoated QDs.[15,51] However, His-coordination onto AuNPs differs from that on QDs in a few aspects. With gold, only partially passivated (*i.e.*, sparsely covered) NPs interact with the proteins, even when smaller ligands (LA or LA-ZW) are used (Figure 2). This implies that these interactions require the availability of unoccupied surface sites on the AuNPs. The ability to implement this metal-affinity self-assembly on AuNPs also depends on the size of the ligand used, with even weaker passivation required for NPs capped with LA-PEG ligands than for their zwitterion-capped counterparts (Figure 2). For instance, NPs prepared using Au:LA-ZW ratios down to 25:1 bind to protein-His, while PEGylated ligands limit protein interactions to NPs prepared with Au:LA-PEG_{750} larger than 50:1 (Figure 2). Fully passivated LA-, LA-ZW-, or LA-PEG-AuNPs do not interact with His-appended proteins even after several rounds of purification (Figures 2 and 3). Finally, self-assembly onto citrate-stabilized AuNPs can be implemented with as prepared dispersions, indicating that citrate groups being very small and weakly bound to the NP surface do not interfere with the metal-His coordination. In comparison, metal-His driven self-assembly of proteins can be implemented with CdSe-ZnS QDs that are fully "passivated" with zwitterion ligands (*i.e.*, compact), but cannot be implemented with QDs photoligated with LA-PEG_{750} (data not shown).[15] We should note that excess free ligands in dispersions of QDs photoligated with LA-ZW is drastically reduced during the phase transfer step, since ligand exchange is also combined with precipitation of the LA-ZW-capped QDs leaving excess free ligands in the solution; they can then be discarded along with the decanted solvent.[42] When metal-His coordination on the AuNPs is permitted, namely for partially passivated NPs, the dissociation constant is overall comparable to that reported for MBP-His_5 self-assembly onto DHLA-QDs.[15]

So, what causes the difference in protein-His self-assembly between the two nanocrystal surfaces, and why does the nature of the metal surface play such

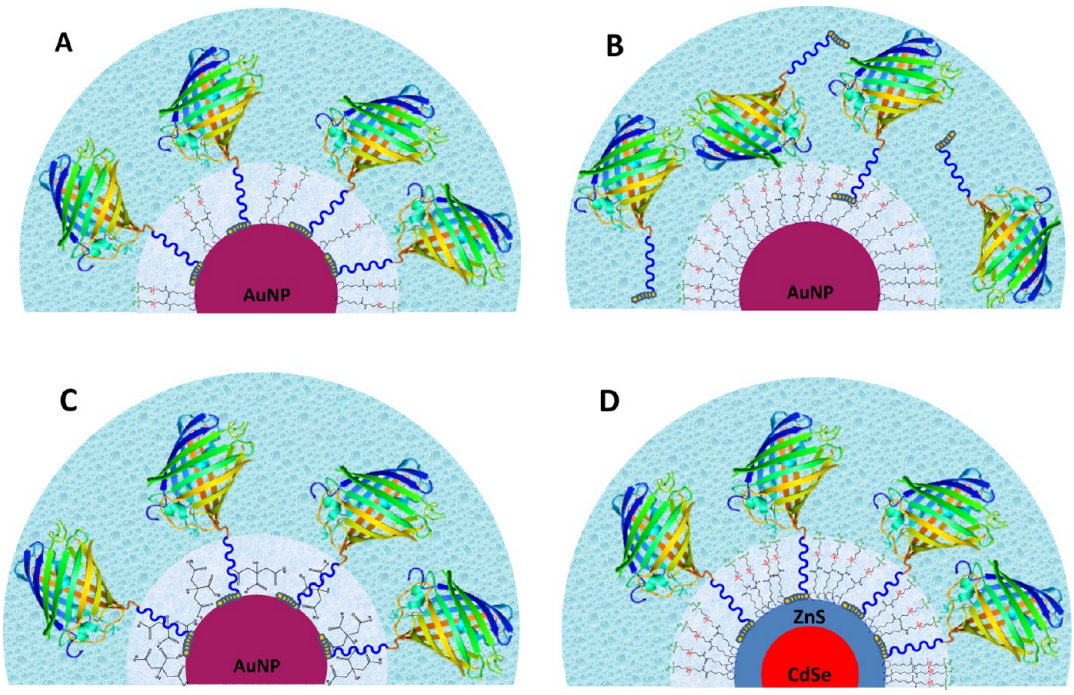

Figure 7. Schematic representation of the mechanistics controlling the interactions involved and competition between the affinity of the ligand-to-NP *versus* that of imidazole to the NP surface. Configurations involving the self-assembly (or lack) of His-protein to AuNPs and Zn-rich QDs upon mixing with (A) partially passivated AuNPs, (B) fully passivated AuNPs, (C) citrate-AuNPs, and (D) CdSe-ZnS core–shell QDs photoligated with LA-ZW ligands.

an important role? We attribute the above results to differences in the nature and strength of the ligand affinity to the gold *versus* semiconducting surfaces of the nanocrystals. Because the metal-histidine driven binding involves direct coordination on the NP surfaces, the imidazole groups must compete with the capping ligands for coordination on the same metal sites. Their ability to access that surface depends on the density of ligands, their sizes, and more importantly, how strongly do those ligands bind to the NP surfaces. Au-thiol coordination is very strong. It is stronger than that of imidazole to Au, and in several instances it has been referred to as covalent bond.[52] Thus, the ability of the imidazole groups to displace or rearrange the density of the bidentate LA-based ligands on the AuNP surface, so that protein can find free enough surface sites to self-assemble on the NP, is limited (Figure 7B). This would allow metal-His self-assembly as a strategy to be applicable only to AuNPs that are partially (or sparsely) capped with LA-ZW ligands, as schematically represented in Figure 7A. Ligands with larger lateral extension such as LA-PEG would require NPs with even less coverage, as the PEG segments would provide additional shielding of the surfaces (Figure 2). In comparison, citrate molecules are small, and their-coordination on the NP surface is weak. This permits easy direct access of the imidazole to the NP surfaces, facilitating the self-assembly of His-tagged proteins and peptides onto the AuNPs (Figure 2C).[31,33] Conversely, the affinity of thiol groups to ZnS-overcoated QDs is weaker than that of thiol-to-Au. This will permit more effective competition of the imidazole with the ligands for coordination onto the QD surface, when close approach is permitted. Thus, when QDs photoligated with LA-ZW ligands are incubated with His-tagged biomolecules, the polyhistidine tail can easily reach the metal-rich surface and induce a rearrangement of the ligand density on the surface, thus permitting self-assembly on the QDs as shown in Figure 3 and schematically represented in Figure 7C. QDs photoligated with LA-PEG ligands present a thicker capping shell, which prevents the imidazoles from reaching the nanocrystal surface, thus preventing the self-assembly of globular proteins onto the nanocrystals.[15,17] Polyhistidine-tagged peptides being less cumbersome can weave through the PEG shell and allow direct access of the imidazole groups to the QD surface, thus promoting QD-peptide conjugation using DHLA-, DHLA-ZW-, and DHLA-PEG-capped QDs.[53,54] Our proposed rationale is supported by the hard/soft acid/base (HSAB) theory as described in Pearson's report,[55] where hard-to-hard and soft-to-soft combinations of molecules or ions bind strongly, because of the polarizability of electron cloud. Here, Au^{1+} and RS^{1-} ions are classified as soft acid and soft base, while the Zn^{2+} and imidazole are considered as borderline acid and base, respectively. Therefore, the Au^{1+} ions should exhibit much higher affinity to RS^{1-} than imidazole groups, while Zn^{2+} would exhibit similar affinities to imidazole and to RS^{1-} groups. This would explain the ability of a polyhistidine tag to competitively rearrange the density of DHLA-based ligands on the QDs. This rationale agrees

with the finding of a recent study by Häkkinen and co-workers who summarized a number of DFT computations of Au−S complexes and concluded that these complexes can be reorganized in ring-like, crown-like, or helical structures. They took into consideration the sp^3 hybridization of the sulfur, where two of the four S(sp^3) hybrid orbitals essentially form "covalent bonds" with the Au(6*s*) electrons.[52] This would imply that the strong interactions between Au^{1+} ions and the dithiol-presenting ligands produce "rigid" ligand arrangement on the NPs, and limit access of the His-tag to the AuNP surfaces.

CONCLUSION

We have presented a molecular characterization of the self-assembly driven by metal-affinity interactions between AuNPs and two proteins expressing an N-terminus polyhistidine tag: maltose binding protein (MBP-His_7) and the fluorescent mCherry protein (mCherry-His_6). In particular, using affinity chromatography combined with energy transfer we explored the effects of varying the nature, size, density, and affinity of the capping ligands on the self-assembly. We found that protein self-assembly onto AuNPs can only be achieved if the NPs were either partially capped with thiol-terminated (strong binding) ligands or stabilized with weakly binding cap such as citrate groups. AuNPs fully passivated with lipoic acid-modified ligands do not permit self-assembly, a result attributed to the high affinity thiol-to-Au coordination. Coordination using thiol group provides a "rigid" ligand attachment onto the nanoparticle, which prevents the imidazoles to compete for coordination to the surface sites. Conversely, with Zn-rich QD surfaces, weaker ligand binding combined with stronger affinity of the imidazoles to the QD can induce a rearrangement of the ligands on the surface, permitting QD-protein-His self-assembly, albeit with only short/compact ligands (*e.g.*, LA and LA-ZW).

Our data clearly showed that the polyhistidine binding to partially passivated LA-ZW-and LA-PEG-AuNPs or citrate-stabilized NPs is strong with a typical dissociation constant $K_d^{-1} \sim 1-5$ nM. This investigation permitted us to develop a fundamental understanding of what drives and controls such metal-His interactions as applied to AuNPs and QDs. Finally, these assemblies of AuNP-protein conjugates with control over the valence and orientation of the proteins on the NP surfaces will be greatly useful in a wide range of applications including *in vitro* protein assays, targeting, and imaging.

EXPERIMENTAL PROCEDURES

Reagents. Tetrachloroauric(III) acid trihydrate ($HAuCl_4 \cdot 3H_2O$) (99.9%), (±-α-lipoic acid) (LA), poly(ethylene glycol) methyl ether ($M_w \sim 750$), methanesulfonyl chloride (99.7%), triphenylphosphine (99%), 4-(*N*,*N*-dimethylamino)pyridine (99%) (DMAP), triethylamine (Et_3N), sodium borohydride ($NaBH_4$), sodium citrate tribasic dihydrate ($C_6H_5Na_3O_7 \cdot 2H_2O$), *N*,*N*-dicylohexylcarbodiimide (DCC), NaOH, KOH, $NaHCO_3$, organic solvents (THF, $CHCl_3$, *etc*), and salts (such as NaCl, Na_2SO_4) were purchased from Sigma Chemicals (St. Louis, MO). Sodium azide (99%), *N*,*N*-dimethyl-1,3-propanediamine (99%), and 1,3-propanesultone (99%) were purchased from Alfa Aesar (Ward Hill, MA). Deuterated solvents were purchased from Cambridge Isotope Laboratories (Andover, MA). The chemicals and solvents were used as purchased unless otherwise specified. Column purification chromatography was performed using silica gel (60 Å, 230−400 mesh, from Bodman Industries, Aston, PA). PD10 columns were purchased from GE Healthcare (Piscataway, NJ).

Instrumentation. The optical absorption measurements were carried out using a Shimadzu UV−vis absorption spectrophotometer (UV 2450 model from Shimadzu). The emission spectra were collected on a Fluorolog-3 spectrometer (HORIBA Jobin Yvon, Inc., Edison, NJ) equipped with a PMT detector. Samples for transmission electron microscopy (TEM) were prepared by drop casting a dispersion of AuNPs onto a fine mesh Cu grid (400 mesh) coated on a holey carbon film and letting it dry; images were collected using a JEOI-2010, 200 kV instrument.

Synthesis of Polyethylene Glycol- and Zwitterion-Modified Lipoic Acid Ligands. We used two sets of lipoic acid (LA)-modified ligands: LA-PEG_{750}-OCH_3, which contains a short PEG moiety ($M_w = 750$) and a terminal methyl ether group, and a more compact zwitterion-modified LA (LA-ZW). They have been synthesized, purified, and characterized following the protocols detailed in previous reports.[40,56−59] The ligands were characterized using ^1H NMR, FT-IR spectroscopy and mass spectrometry techniques.

One Phase Growth of Lipoic Acid-, Lipoic Acid-PEG- and Lipoic Acid-Zwitterion-Capped AuNPs. The growth reaction relied on the reduction of Au(III) using sodium borohydride in the presence of the oxidized form of the ligands, LA, LA-ZW, or LA-PEG_{750}-OCH_3, following the rationales described in the literature.[43,44] In a typical reaction, 12 μL of 1.5 mM ligand solution was first dissolved in 5 mL of deionized water, followed by the addition of 32 μL of 50 mM stock solution of $HAuCl_4 \cdot 3H_2O$ in water; this corresponds to Au:ligand molar ratio ~90:1.[43] The mixture was stirred for 30 min, and then 45 μL of 290 mM $NaBH_4$ solution in water was added dropwise with vigorous stirring. The reaction mixture was then left stirring for 3 h at room temperature. For the extra passivation step, additional amounts of LA, LA-ZW, or LA-PEG_{750}-OCH_3 ligands were added to the AuNP solution and further stirred for 3 h; the final Au-to-ligand ratios used, including passivation, were 90:1, 50:1, 25:1, 5:1, 2:1, and 1:1. The dispersions were purified from free reagents (excess free ligands and precursor) by applying three cycles of centrifugation/filtration using a membrane filtration device (Millipore) with a molecular weight cutoff of 50 kDa. The resulting dispersions were stored at room temperature until further use. We should note that because LA was insoluble in pure water, a stock solution of the ligand in methanol (at 1.5 mM) was first prepared. Then, 12 μL of this solution was used to carry out the growth reaction in water as described above.

Growth of Citrate-Stabilized AuNPs. For this, citrate-stabilized 5 nm AuNPs were first grown following rationales reported in the literature.[60,61] Briefly, 250 μL of 50 mM aqueous solution of $HAuCl_4 \cdot 3H_2O$ was added to 50 mL of water. After stirring for ~1 min, 1 mL of a 38.8 mM sodium citrate solution in water was added. In parallel, 100 μL of 200 mM $NaBH_4$ was mixed with 900 μL of 38.8 mM sodium citrate solution and rapidly injected in the above flask containing Au precursor and ligands. The reaction mixture was stirred for an additional 2 h and then purified using a membrane filtration device (Millipore) as above.

Preparation of LA-ZW-Functionalized AuNPs *via* Ligand Exchange. Citrate-stabilized AuNPs prepared above were purified and

mixed with 800 equiv of LA-ZW ligands, the solution pH was adjusted to pH 10, and then the mixture was left stirring for 24 h at room temperature. Then, the AuNP dispersions were subjected to further purification (to remove excess free ligands) by applying one, two, or three rounds of concentration/dilution using a membrane filtration device (with a cutoff M_w = 50 kDa), as described in the main text above. Estimates of the NP concentration were determined using the extinction coefficient $\varepsilon_{520} = 1.10 \times 10^7$ M^{-1} cm^{-1} for 5 nm AuNPs (Sigma Aldrich).[43]

Expression and Purification of Polyhistidine-Tagged Maltose Binding Protein: MBP-His$_7$. Protein expression was carried out using a pMalE3 plasmid engineered to express a maltose binding protein (MBP) sequence with a seven-histidine tag (His_7) MHHHHHHHSTS- at the N-terminus.[62] This plasmid was provided by Timothy A. Cross's laboratory at the Florida State University. The plasmid was transformed into *Escherichia coli* bacterial cells (BL21 strain, from Analytical Core Facility, Florida State University), plated on LB/Ampicillin Petri dish, and left overnight at 37 °C. Single colonies were plucked from the plates and dispersed into Luria−Bertani (LB) media to start overnight cultures at 37 °C while shacking at 200 rpm. Then, the saturated culture was inoculated in LB media using a volume ratio of culture-to-LB of 1:100. When the OD_{600} reached 0.6, MBP expression was induced by the addition of 0.4 mM isopropyl β-D-1-thiogalactopyranoside (Fisher Scientific). After 6 h of induction, the culture was harvested in binding buffer (25 mM Tris-HCl, pH 8.0, 500 mM NaCl, 10 mM imidazole) and lysed using a microfluidizer. The lysate was centrifuged for 15 min at 15 000 rpm, and the polyhistidine-tagged protein in the supernatant was purified using a high-capacity nickel-IMAC resin (Fisher Scientific) in binding buffer containing 250 mM imidazole. Fractions were concentrated using a membrane filtration device (Centricon-Millipore Amicon-Ultra-15 Centrifugal Filter Units, cutoff M_w = 10 kDa). The obtained protein was then purified using anion exchange HPLC (MonoQ, GE Healthcare, Piscataway, NJ). The purified proteins were diafiltrated into PBS buffer (10 mM sodium phosphate, 137 mM NaCl, 2 mM KCl, pH 7.4) using Centricon units and stored at 4 °C.

Expression and Purification of Polyhistidine-Tagged mCherry Fluorescent Protein: mCherry-His$_6$. The mCherry-His_6 protein was derived from pBAD plasmid provided by Mike Davidson's laboratory at the National High Magnetic Field Laboratory (NHMFL, Florida State University). This plasmid was expressed in TOP10 competent strain (*Escherichia coli*), and the expression was induced with 0.2% L-arabinose. The polyhistidine sequence appended to N-terminus of the mCherry was used for protein purification using a high-capacity nickel-IMAC resin (Fisher Scientific). The purification and the characterization steps are similar to those described above for the MBP-His_7.

Self-Assembly of AuNP-Protein-His Conjugates. Different sample configurations were prepared and tested. In a typical sample preparation, 5 μL of His-tagged protein (80 μM stock solution of MBP-His_7 or mCherry-His_6) was first added to an eppendorf tube containing 95 μL of PBS buffer. In a separate tube, 50 μL of a stock solution of AuNPs (0.8 μM) was diluted in PBS buffer to a total volume of 100 μL. The contents of the tubes were mixed gently and left to incubate at 4 °C for 45 min. The molar ratio of AuNP-to-MBP-His_7 was maintained at 1:10 in all cases, while the ratio for AuNP-to-mCherry-His_6 was varied from 1:2 to 1:10. The concentrations of both proteins were determined using the extinction coefficients: 71000 M^{-1} cm^{-1} at 587 nm for mCherry and 35870 M^{-1} cm^{-1} at 280 nm for MBP, respectively.[63,64] The dispersions of AuNP-mCherry assemblies were used to investigate the effects of AuNP fluorescent quenching of mCherry emission and its dependence on the conjugate valence. Binding of MBP-His_7 onto the AuNPs relied on a visual assay based on the specific binding of MBP to amylose (in a gel column loaded with amylose), followed by release with soluble maltose. Briefly, 1.5−2 mL of amylose stock gel was loaded onto a 10 mL capacity column and washed three times with 10 mL of PBS buffer. The AuNP and MPB-His_7 mixture was then loaded onto the column and washed with PBS buffer pH = 7.4 (4 times, 5 mL each). When AuNP-MPB-His_7 conjugates are formed in the solution, a pink colored band, promoted by the binding of MBP in the conjugate, builds up on the top of the column; the band is not affected by multiple washes with buffer. Adding 5 mL of a 20 mM solution of D-(+)-maltose to the column progressively displaced the pink band (AuNP-MBP conjugates), which was collected and further characterized. When AuNP to MBP-His_7 conjugation does not take place, the pink solution of the AuNPs immediately eluted after loading onto the amylose column.

Kinetics of AuNPs-mCherry Self-Assembly in Solution. Monitoring the kinetics of the self-assembly between partially passivated LA-, LA-ZW-, LA-PEG-capped, and citrate-capped AuNPs and mCherry-His_6 in solution was carried out following the rationales we previously detailed for the self-assembly of Cy5-labeled MBP-His_5 onto DHLA-capped QDs.[15] Here the protein itself provided the necessary absorption and emission signatures. Briefly, varying amounts of mCherry-His_6 were dispersed in 10 mM phosphate buffer solution (pH = 7.4) at concentrations ranging from 1 to 60 nM. For each concentration, the dispersion was loaded in a quartz cuvette (optical path = 5 mm), the sample excited at the absorption maximum of the mCherry at 587 nm, and the time-progression of the mCherry PL (at the maximum 610 nm window) was collected using a Fluorolog-3 spectrometer. More precisely, following an initial acquisition period of the PL signal of ~50 s from the pure protein solution (without AuNPs), to ensure that mCherry PL signal was stable, the AuNPs were added (at a fixed mCherry-to-AuNP molar ratio of 1) mixed, and a series of 2 s signal acquisitions was collected over a period of 450 s. This allowed a continuous monitoring of the self-assembly kinetics, where changes in the mCherry quenching induced by the bound AuNP provided a time-dependent progression of the self-assembly. As the number of self-assembled AuNP-mCherry conjugates in the sample increased, the ensemble mCherry PL systematically decreased due to energy transfer quenching. The kinetic of AuNP-mCherry self-assembly became more rapid by increasing the reagent concentrations in the sample. Analysis of these kinetics data provided values for the apparent binding rate, k_{app}, *versus* concentration, which were further exploited to extract an estimate for the dissociation constant, K_d^{-1}, for these AuNP-mCherry assemblies.

Conflict of Interest: The authors declare no competing financial interest.

Acknowledgment. We thank FSU and the National Science Foundation (NSF-CHE, #1058957) for financial support. We also thank Xin Ji and Anshika Kapur for the helpful discussions. The TEM experiments were carried out at the FSU TEM facility and funded and supported by the Florida State University Research Foundation, the National High Magnetic Field Laboratory (NSF-DMR-0654118), and the State of Florida.

Supporting Information Available: Additional affinity chromatography tests and fluorescence data with LA-PEG-AuNPs and kinetics of mCherry binding to LA-AuNPs. This information is available free of charge *via* the Internet at http://pubs.acs.org.

REFERENCES AND NOTES

1. Alivisatos, P. The Use of Nanocrystals in Biological Detection. *Nat. Biotechnol.* **2004**, *22*, 47–52.
2. Michalet, X.; Pinaud, F.; Bentolila, L.; Tsay, J.; Doose, S.; Li, J.; Sundaresan, G.; Wu, A.; Gambhir, S.; Weiss, S. Quantum Dots for Live Cells, *in Vivo* Imaging, and Diagnostics. *Science* **2005**, *307*, 538–544.
3. Biju, V.; Itoh, T.; Anas, A.; Sujith, A.; Ishikawa, M. Semiconductor Quantum Dots and Metal Nanoparticles: Syntheses, Optical Properties, and Biological Applications. *Anal. Bioanal. Chem.* **2008**, *391*, 2469–2495.
4. De, M.; Ghosh, P. S.; Rotello, V. M. Applications of Nanoparticles in Biology. *Adv. Mater.* **2008**, *20*, 4225–4241.
5. Zrazhevskiy, P.; Sena, M.; Gao, X. H. Designing Multifunctional Quantum Dots for Bioimaging, Detection, and Drug Delivery. *Chem. Soc. Rev.* **2010**, *39*, 4326–4354.
6. Sperling, R. A.; Parak, W. J. Surface Modification, Functionalization and Bioconjugation of Colloidal Inorganic Nanoparticles. *Philos. Trans. R. Soc., A* **2010**, *368*, 1333–1383.

7. Mattoussi, H.; Palui, G.; Na, H. B. Luminescent Quantum Dots as Platforms for Probing *in Vitro* and *in Vivo* Biological Processes. *Adv. Drug Delivery Rev.* **2012**, *64*, 138–166.
8. Pelaz, B.; Jaber, S.; de Aberasturi, D. J.; Wulf, V.; Aida, T.; de la Fuente, J. M.; Feldmann, J.; Gaub, H. E.; Josephson, L.; Kagan, C. R.; *et al.* The State of Nanoparticle-Based Nanoscience and Biotechnology: Progress, Promises, and Challenges. *ACS Nano* **2012**, *6*, 8468–8483.
9. Medintz, I. L.; Uyeda, H. T.; Goldman, E. R.; Mattoussi, H. Quantum Dot Bioconjugates for Imaging, Labelling and Sensing. *Nat. Mater.* **2005**, *4*, 435–446.
10. Somers, R. C.; Bawendi, M. G.; Nocera, D. G. CdSe Nanocrystal Based Chem-/Bio-sensors. *Chem. Soc. Rev.* **2007**, *36*, 579–591.
11. Winnik, F. M.; Maysinger, D. Quantum Dot Cytotoxicity and Ways To Reduce It. *Acc. Chem. Res.* **2012**, *46*, 672–680.
12. Sapsford, K. E.; Algar, W. R.; Berti, L.; Gemmill, K. B.; Casey, B. J.; Oh, E.; Stewart, M. H.; Medintz, I. L. Functionalizing Nanoparticles with Biological Molecules: Developing Chemistries that Facilitate Nanotechnology. *Chem. Rev.* **2013**, *113*, 1904–2074.
13. Shen, H.; Jawaid, A. M.; Snee, P. T. Poly(ethylene glycol) Carbodiimide Coupling Reagents for the Biological and Chemical Functionalization of Water-Soluble Nanoparticles. *ACS Nano* **2009**, *3*, 915–923.
14. Guo, W. Z.; Li, J. J.; Wang, Y. A.; Peng, X. G. Conjugation Chemistry and Bioapplications of Semiconductor Box Nanocrystals Prepared *Via* Dendrimer Bridging. *Chem. Mater.* **2003**, *15*, 3125–3133.
15. Sapsford, K. E.; Pons, T.; Medintz, I. L.; Higashiya, S.; Brunel, F. M.; Dawson, P. E.; Mattoussi, H. Kinetics of Metal-Affinity Driven Self-Assembly Between Proteins or Peptides and CdSe-ZnS Quantum Dots. *J. Phys. Chem. C* **2007**, *111*, 11528–11538.
16. Goldman, E. R.; Medintz, I. L.; Hayhurst, A.; Anderson, G. P.; Mauro, J. M.; Iverson, B. L.; Georgiou, G.; Mattoussi, H. Self-Assembled Luminescent CdSe-ZnS Quantum Dot Bioconjugates Prepared Using Engineered Poly-histidine Terminated Proteins. *Anal. Chim. Acta* **2005**, *534*, 63–67.
17. Dennis, A. M.; Sotto, D. C.; Mei, B. C.; Medintz, I. L.; Mattoussi, H.; Bao, G. Surface Ligand Effects on Metal-Affinity Coordination to Quantum Dots: Implications for Nanoprobe
Self-Assembly. *Bioconjugate Chem.* **2010**, *21*, 1160–1170.
18. Burda, C.; Chen, X. B.; Narayanan, R.; El-Sayed, M. A. Chemistry and Properties of Nanocrystals of Different Shapes. *Chem. Rev.* **2005**, *105*, 1025–1102.
19. Daniel, M. C.; Astruc, D. Gold Nanoparticles: Assembly, Supramolecular Chemistry, Quantum-Size-Related Properties, and Applications Toward Biology, Catalysis, and Nanotechnology. *Chem. Rev.* **2004**, *104*, 293–346.
20. Saha, K.; Agasti, S. S.; Kim, C.; Li, X. N.; Rotello, V. M. Gold Nanoparticles in Chemical and Biological Sensing. *Chem. Rev.* **2012**, *112*, 2739–2779.
21. Oh, E.; Hong, M. Y.; Lee, D.; Nam, S. H.; Yoon, H. C.; Kim, H. S. Inhibition Assay of Biomolecules Based on Fluorescence Resonance Energy Transfer (FRET) Between Quantum Dots and Gold Nanoparticles. *J. Am. Chem. Soc.* **2005**, *127*, 3270–3271.
22. Mitchell, G. P.; Mirkin, C. A.; Letsinger, R. L. Programmed Assembly of DNA Functionalized Quantum Dots. *J. Am. Chem. Soc.* **1999**, *121*, 8122–8123.
23. Mirkin, C. A.; Letsinger, R. L.; Mucic, R. C.; Storhoff, J. J. A DNA-based Method for Rationally Assembling Nanoparticles Into Macroscopic Materials. *Nature* **1996**, *382*, 607–609.
24. Elghanian, R.; Storhoff, J. J.; Mucic, R. C.; Letsinger, R. L.; Mirkin, C. A. Selective Colorimetric Detection of Polynucleotides Based on the Distance-Dependent Optical Properties of Gold Nanoparticles. *Science* **1997**, *277*, 1078–1081.
25. Singh, M. P.; Strouse, G. F. Involvement of the LSPR Spectral Overlap for Energy Transfer between a Dye and Au Nanoparticle. *J. Am. Chem. Soc.* **2010**, *132*, 9383–9391.
26. Aldeek, F.; Ji, X.; Mattoussi, H. Quenching of Quantum Dot Emission by Fluorescent Gold Clusters: What It Does and Does Not Share with the Förster Formalism. *J. Phys. Chem. C* **2013**, *117*, 15429–15437.
27. Pons, T.; Medintz, I. L.; Sapsford, K. E.; Higashiya, S.; Grimes, A. F.; English, D. S.; Mattoussi, H. On the Quenching of Semiconductor Quantum Dot Photoluminescence by Proximal Gold Nanoparticles. *Nano Lett.* **2007**, *7*, 3157–3164.
28. Mayilo, S.; Kloster, M. A.; Wunderlich, M.; Lutich, A.; Klar, T. A.; Nichtl, A.; Kurzinger, K.; Stefani, F. D.; Feldmann, J. Long-Range Fluorescence Quenching by Gold Nanoparticles in a Sandwich Immunoassay for Cardiac Troponin T. *Nano Lett.* **2009**, *9*, 4558–4563.
29. Griffin, J.; Singh, A. K.; Senapati, D.; Rhodes, P.; Mitchell, K.; Robinson, B.; Yu, E.; Ray, P. C. Size- and Distance-Dependent Nanoparticle Surface-Energy Transfer (NSET) Method for Selective Sensing of Hepatitis C Virus RNA. *Chem.—Eur. J.* **2009**, *15* (2), 342–351.
30. Sen, T.; Patra, A. Resonance Energy Transfer from Rhodamine 6G to Gold Nanoparticles by Steady-State and Time-Resolved Spectroscopy. *J. Phys. Chem. C* **2008**, *112*, 3216–3222.
31. Kogot, J. M.; England, H. J.; Strouse, G. F.; Logan, T. M. Single Peptide Assembly onto a 1.5 nm Au Surface *via* a Histidine Tag. *J. Am. Chem. Soc.* **2008**, *130*, 16156–16156.
32. Kogot, J. M.; Parker, A. M.; Lee, J.; Blaber, M.; Strouse, G. F.; Logan, T. M. Analysis of the Dynamics of Assembly and Structural Impact for a Histidine Tagged FGF1−1.5 nm Au Nanoparticle Bioconjugate. *Bioconjugate Chem.* **2009**, *20*, 2106–2113.
33. Petryayeva, E.; Krull, U. J. Quantum Dot and Gold Nanoparticle Immobilization for Biosensing Applications using Multidentate Imidazole Surface Ligands. *Langmuir* **2012**, *28*, 13943–13951.
34. Duan, H. W.; Kuang, M.; Wangi, Y. A. Quantum Dots with Multivalent and Compact Polymer Coatings for Efficient Fluorescence Resonance Energy Transfer and Self-Assembled Biotagging. *Chem. Mater.* **2010**, *22*, 4372–4378.
35. Medintz, I. L.; Sapsford, K. E.; Clapp, A. R.; Pons, T.; Higashiya, S.; Welch, J. T.; Mattoussi, H. Designer Variable Repeat Length Polypeptides as Scaffolds for Surface Immobilization of Quantum Dots. *J. Phys. Chem. B* **2006**, *110*, 10683–10690.
36. Clapp, A. R.; Medintz, I. L.; Mauro, J. M.; Fisher, B. R.; Bawendi, M. G.; Mattoussi, H. Fluorescence Resonance Energy Transfer Between Quantum Dot Donors and Dye-Labeled Protein Acceptors. *J. Am. Chem. Soc.* **2004**, *126*, 301–310.
37. Wang, J. H.; Xia, J. Preferential Binding of a Novel Polyhistidine Peptide Dendrimer Ligand on Quantum Dots Probed by Capillary Electrophoresis. *Anal. Chem.* **2011**, *83*, 6323–6329.
38. Susumu, K.; Oh, E.; Delehanty, J. B.; Blanco-Canosa, J. B.; Johnson, B. J.; Jain, V.; Hervey, W. J.; Algar, W. R.; Boeneman, K.; Dawson, P. E.; *et al.* Multifunctional Compact Zwitterionic Ligands for Preparing Robust Biocompatible Semiconductor Quantum Dots and Gold Nanoparticles. *J. Am. Chem. Soc.* **2011**, *133*, 9480–9496.
39. Medintz, I. L.; Clapp, A. R.; Mattoussi, H.; Goldman, E. R.; Fisher, B.; Mauro, J. M. Self-Assembled Nanoscale Biosensors Based on Quantum Dot FRET Donors. *Nat. Mater.* **2003**, *2*, 630–638.
40. Zhan, N.; Palui, G.; Grise, H.; Tang, H.; Alabugin, I.; Mattoussi, H. Combining Ligand Design with Photoligation to Provide Compact, Colloidally Stable, and Easy to Conjugate Quantum Dots. *ACS Appl. Mater. Interfaces* **2013**, *5*, 2861–2869.
41. Boeneman, K.; Mei, B. C.; Dennis, A. M.; Bao, G.; Deschamps, J. R.; Mattoussi, H.; Medintz, I. L. Sensing Caspase 3 Activity with Quantum Dot-Fluorescent Protein Assemblies. *J. Am. Chem. Soc.* **2009**, *131*, 3828–3829.
42. Palui, G.; Avellini, T.; Zhan, N.; Pan, F.; Gray, D.; Alabugin, I.; Mattoussi, H. Photoinduced Phase Transfer of Luminescent Quantum Dots to Polar and Aqueous Media. *J. Am. Chem. Soc.* **2012**, *134*, 16370–16378.
43. Oh, E.; Susumu, K.; Goswami, R.; Mattoussi, H. One-Phase Synthesis of Water-Soluble Gold Nanoparticles with

Control over Size and Surface Functionalities. *Langmuir* **2010**, *26*, 7604–7613.
44. Aldeek, F.; Muhammed, M. A.; Palui, G.; Zhan, N.; Mattoussi, H. Growth of Highly Fluorescent Polyethylene Glycol- and Zwitterion-Functionalized Gold Nanoclusters. *ACS Nano* **2013**, *7*, 2509–2521.
45. Murray, C. B.; Norris, D. J.; Bawendi, M. G. Synthesis and Characterization of Nearly Monodisperse Cde (E = S, Se, Te) Semiconductor Nanocrystallites. *J. Am. Chem. Soc.* **1993**, *115*, 8706–8715.
46. Dabbousi, B. O.; RodriguezViejo, J.; Mikulec, F. V.; Heine, J. R.; Mattoussi, H.; Ober, R.; Jensen, K. F.; Bawendi, M. G. (CdSe)ZnS Core-Shell Quantum Dots: Synthesis and Characterization of a Size Series of Highly Luminescent Nanocrystallites. *J. Phys. Chem. B* **1997**, *101*, 9463–9475.
47. Clapp, A. R.; Goldman, E. R.; Mattoussi, H. Capping of CdSe-ZnS Quantum Dots with DHLA and Subsequent Conjugation with Proteins. *Nat. Protoc.* **2006**, *1*, 1258–1266.
48. Qu, L. H.; Peng, Z. A.; Peng, X. G. Alternative Routes Toward High Quality CdSe Nanocrystals. *Nano Lett.* **2001**, *1*, 333–337.
49. Reiss, P.; Bleuse, J.; Pron, A. Highly Luminescent CdSe/ZnSe Core/Shell Nanocrystals of Low Size Dispersion. *Nano Lett.* **2002**, *2*, 781–784.
50. Vijayendran, R. A.; Ligler, F. S.; Leckband, D. E. A Computational Reaction-Diffusion Model for the Analysis of Transport-Limited Kinetics. *Anal. Chem.* **1999**, *71*, 5405–5412.
51. Liu, W. H.; Greytak, A. B.; Lee, J.; Wong, C. R.; Park, J.; Marshall, L. F.; Jiang, W.; Curtin, P. N.; Ting, A. Y.; Nocera, D. G.; *et al.* Compact Biocompatible Quantum Dots *via* RAFT-Mediated Synthesis of Imidazole-Based Random Copolymer Ligand. *J. Am. Chem. Soc.* **2010**, *132*, 472–483.
52. Hakkinen, H. The Gold-Sulfur Interface at the Nanoscale. *Nat. Chem.* **2012**, *4*, 443–455.
53. Delehanty, J. B.; Medintz, I. L.; Pons, T.; Brunel, F. M.; Dawson, P. E.; Mattoussi, H. Self-Assembled Quantum Dot-Peptide Bioconjugates for Selective Intracellular Delivery. *Bioconjugate Chem.* **2006**, *17*, 920–927.
54. Medintz, I. L.; Stewart, M. H.; Trammell, S. A.; Susumu, K.; Delehanty, J. B.; Mei, B. C.; Melinger, J. S.; Blanco-Canosa, J. B.; Dawson, P. E.; Mattoussi, H. Quantum-Dot/Dopamine Bioconjugates Function as Redox Coupled Assemblies for *in Vitro* and Intracellular pH Sensing. *Nat. Mater.* **2010**, *9*, 676–684.
55. Pearson, R. G. Hard and Soft Acids and Bases. *J. Am. Chem. Soc.* **1963**, *85*, 3533–3539.
56. Mei, B. C.; Susumu, K.; Medintz, I. L.; Delehanty, J. B.; Mountziaris, T. J.; Mattoussi, H. Modular Poly(ethylene glycol) Ligands for Biocompatible Semiconductor and Gold Nanocrystals with Extended pH and Ionic Stability. *J. Mater. Chem.* **2008**, *18*, 4949–4958.
57. Susumu, K.; Mei, B. C.; Mattoussi, H. Multifunctional Ligands Based on Dihydrolipoic Acid and Polyethylene Glycol to Promote Biocompatibility of Quantum Dots. *Nat. Protoc.* **2009**, *4*, 424–436.
58. Susumu, K.; Uyeda, H. T.; Medintz, I. L.; Pons, T.; Delehanty, J. B.; Mattoussi, H. Enhancing the Stability and Biological Functionalities of Quantum Dots *via* Compact Multifunctional Ligands. *J. Am. Chem. Soc.* **2007**, *129*, 13987–13996.
59. Park, J.; Nam, J.; Won, N.; Jin, H.; Jung, S.; Jung, S.; Cho, S. H.; Kim, S. Compact and Stable Quantum Dots with Positive, Negative, or Zwitterionic Surface: Specific Cell Interactions and Non-Specific Adsorptions by the Surface Charges. *Adv. Funct. Mater.* **2011**, *21*, 1558–1566.
60. Brown, K. R.; Walter, D. G.; Natan, M. J. Seeding of Colloidal Au Nanoparticle Solutions. 2. Improved Control of Particle Size and Shape. *Chem. Mater.* **2000**, *12*, 306–313.
61. Tournebize, J.; Boudier, A.; Sapin-Minet, A.; Maincent, P.; Leroy, P.; Schneider, R. Role of Gold Nanoparticles Capping Density on Stability and Surface Reactivity to Design Drug Delivery Platforms. *ACS Appl. Mater. Interfaces* **2012**, *4*, 5790–5799.
62. Hu, J.; Qin, H. J.; Gao, F. P.; Cross, T. A. A Systematic Assessment of Mature MBP in Membrane Protein Production: Overexpression, Membrane Targeting and Purification. *Protein Expression Purif.* **2011**, *80*, 34–40.
63. Medintz, I. L.; Pons, T.; Susumu, K.; Boeneman, K.; Dennis, A. M.; Farrell, D.; Deschamps, J. R.; Melinger, J. S.; Bao, G.; Mattoussi, H. Resonance Energy Transfer Between Luminescent Quantum Dots and Diverse Fluorescent Protein Acceptors. *J. Phys. Chem. C* **2009**, *113*, 18552–18561.
64. Dennis, A. M.; Bao, G. Quantum Dot−Fluorescent Protein Pairs as Novel Fluorescence Resonance Energy Transfer Probes. *Nano Lett.* **2008**, *8*, 1439–1445.